Supporting Information

Enhancing the proton conduction in α-zirconium phosphate nanoplates by amine intercalation

Zhiwei Wang[a,b*], Zihao Song[a], Wenqi Jiang[a], Jin Zhu[a], Xianfei Luo[a,c], Yuchen Li[a], Wenbin Zhu[a], Gan Jin[a,b], Huayu Tang[d], Xing Gao[a] and Xueli Liu[a*]

a. School of Materials Science and Chemical Engineering, Chuzhou University, 1 West Huifeng Road, Chuzhou 23900, China

b. Anhui Generic Technology Research Center for Semiconductor and Intelligent Sensing Industries, 1 West Huifeng Road, Chuzhou 23900, China

c. Chuzhou Research Institute of Anhui University, 666 East Hongwu Road, Chuzhou 23900, China

d. School of Computer and Information Engineering, Chuzhou University, 1 West Huifeng Road, Chuzhou 23900, China

* E-mail address: zwwang@chzu.edu.cn; n_xueli@163.com

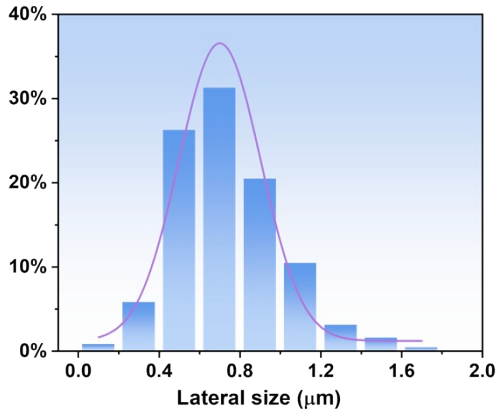

Figure S1 Lateral size distribution of α-ZrP nanoplates showing a mean lateral size of ca. 700 nm.

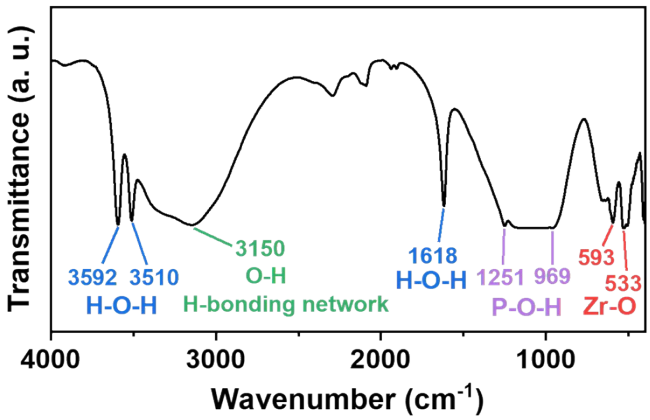

Figure S2 FT-IR spectrum of α-ZrP nanoplates.

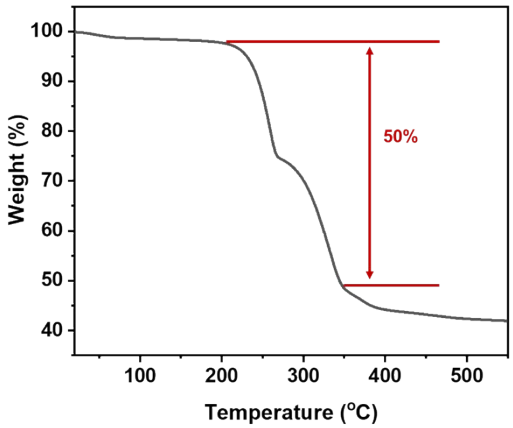

Figure S3 TGA curve of α-ZrP-DDA (1:4). The weight loss occurring from 200°C to 350°C is expected to be the decomposition of DDA (~50%), which proceeds in two distinct steps. The first (200-270°C) and second (270-350°C) stages can be attributed to the free and anchored DDA within the galleries, respectively.

Table S1 The comparisons of the proton conductivities between α-ZrP-DDA (1:4) and proton conductors based on ZrP with different intercalants.

Materials	T (K)	RH	σ (S cm^{-1})	Ref
α-ZrP-DDA (1:4)	303	98%	1.11×10^{-4}	This work
ZrP·*x*PrN·*n*H_2O	293	90%	1.20×10^{-3}	1
ZPS2	295	100%	2.80×10^{-3}	2
α-ZrP 0.95 (imidazole)	393	0%	1.90×10^{-7}	3
α-ZrP 0.75 (pyrazole)	393	0%	1.40×10^{-6}	4
Al_{13}-ZrP	298	60%	3.00×10^{-4}	5
ZrP/[EMIM][ESO_4]	298	/	2.26×10^{-2}	
ZrP/[BMIM][DCA]	298	/	1.36×10^{-2}	6
ZrP/[BMIM][OTF]	298	/	1.16×10^{-2}	

Table S2 Summarization of the proton conductivities of α-ZrP-DDA (1:4) at different temperature and 98% RH.

T (K)	R (Ω)	σ (S cm^{-1})
293	1310	9.72×10^{-5}
303	1146	1.11×10^{-4}
313	996	1.28×10^{-4}
323	843	1.51×10^{-4}
333	726	1.75×10^{-4}
343	614	2.07×10^{-4}
353	530	2.40×10^{-4}
363	465	2.74×10^{-4}

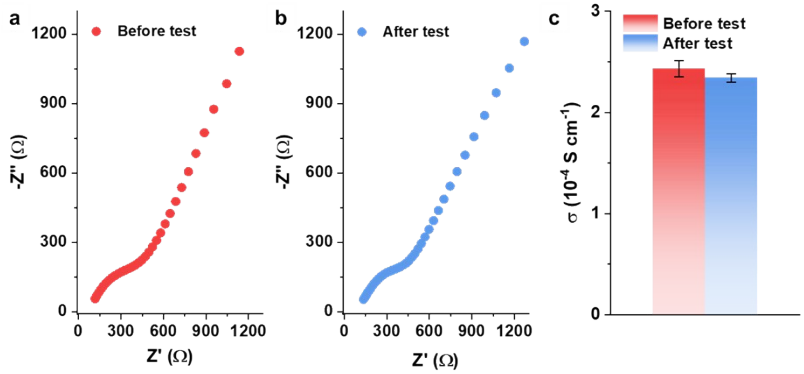

Figure S4 Nyquist plots of α-ZrP-DDA (1:4) at 353 K and 98% RH (a) before and (b) after a two-month interval following the initial test. (c) Comparison of proton conductivity of α-ZrP-DDA (1:4) nanoplates at 353 K and 98% RH before and after the test. Each error bar indicates the standard deviation of the proton conductivity for 5 experimental replicates.

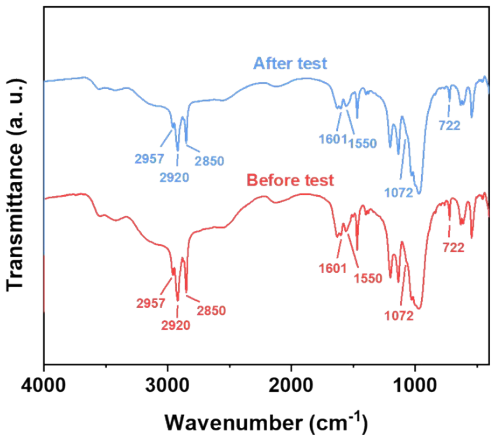

Figure S5 FT-IR spectra of α-ZrP-DDA (1:4) before and after proton conductivity test.

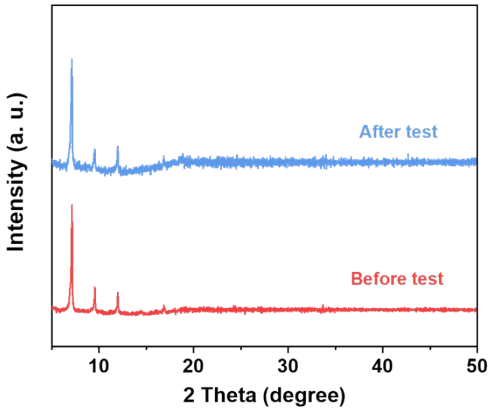

Figure S6 XRD patterns of α-ZrP-DDA (1:4) before and after proton conductivity test.

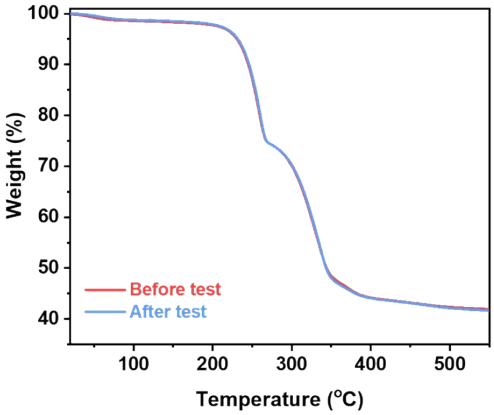

Figure S7 TGA curves of α-ZrP-DDA (1:4) before and after proton conductivity test.

Table S3 Summarization of the proton conductivities of α-ZrP-DDA (1:4) at different RH and 303 K.

RH	R (Ω)	σ (S cm^{-1})
98%	1146	1.11×10^{-4}
84%	7050	1.81×10^{-5}
75%	3.06×10^{4}	4.16×10^{-6}
68%	1.42×10^{5}	8.97×10^{-7}
57%	4.49×10^{7}	2.84×10^{-9}

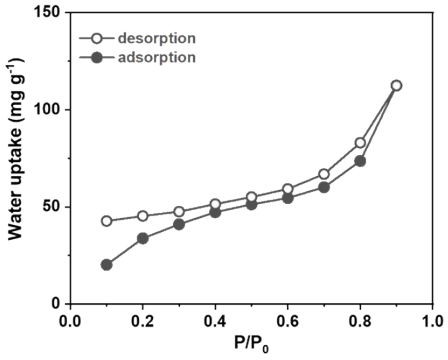

Figure S8 Water adsorption-desorption isotherm of α-ZrP-DDA (1:4) nanoplates collected at 298 K.

Figure S9 Photograph of a humidity sensor based on α-ZrP-DDA (1:4).

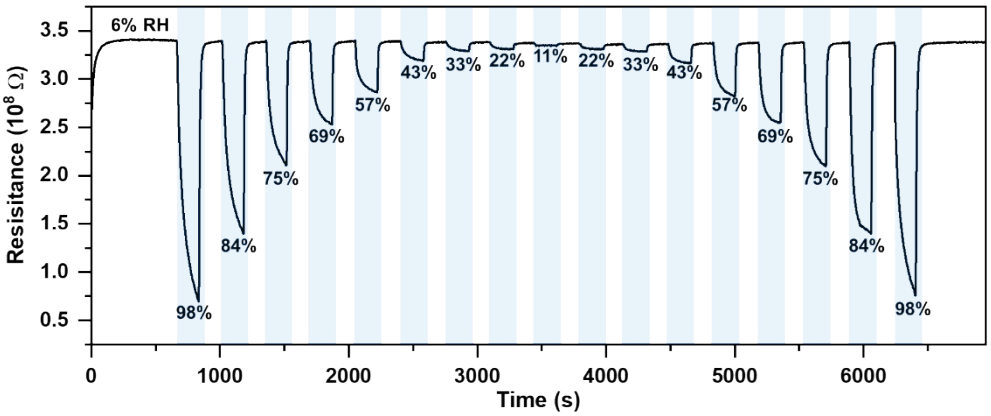

Figure S10 Dynamic response-recovery curve of α-ZrP-DDA (1:4) toward different RHs. The sensing mechanism of the sensor is similar to that of other humidity sensors based on ion-conducting materials.[7, 8] When RH is low, only a small number of water molecules are adsorbed, which causes the protons to transfer through physical migration, leading to a relatively low proton conductivity. At elevated RHs, the presence of expanded interlayer spacing and unanchored, free DDA molecules facilitates the adsorption of more water molecules, resulting in an increase in carrier concentration and the formation of hydrogen-bonding networks. These consequently boost the transportation of protons via rapid and continuous breaking and reformation of hydrogen bonds, which leads to greatly enhanced proton conductivity and, subsequently, a high sensing response.

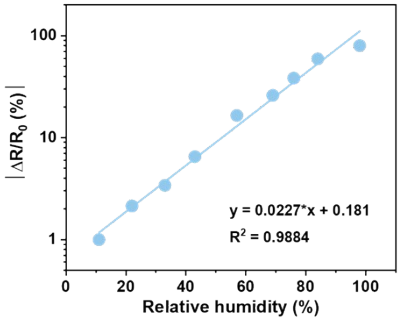

Figure S11 Fitting of the absolute value of responses as a function of RH.

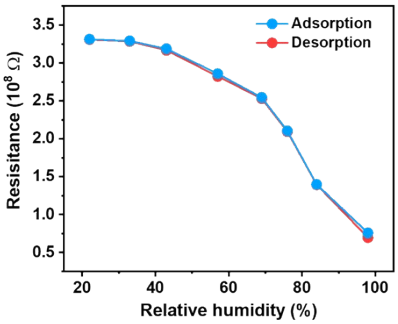

Figure S12 Hysteresis characteristic of *α*-ZrP-DDA (1:4).

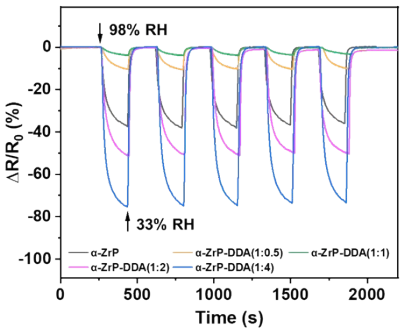

Figure S13 Response curves of α-ZrP and DDA-intercalated α-ZrPs to 98% RH, with a background RH of 33%. Notably, the α-ZrP-DDA (1:4) showed significantly larger responses (-79.8%) than the other materials (*i.e.*, α-ZrP: -39.1%, α-ZrP-DDA (1:0.5): -10.8%, α-ZrP-DDA (1:1): -3.9% and α-ZrP-DDA (1:2): -52.8%).

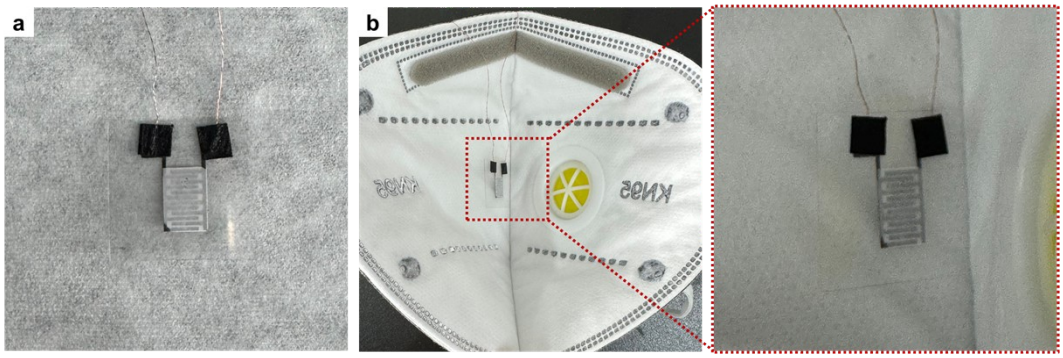

Figure S14 Photographs of a typical breath sensing device (a) connected to two copper wires and (b) attached on the inside surface of a mask.

References

1. M. Casciola, U. Constantino and S. D'Amico, *Solid State Ionics*, 1986, **22**, 127-133.
2. Z. P. Xu, Y. Jin, J. C. Diniz da Costa and G. Q. Lu, *Solid State Ionics*, 2008, **178**, 1654-1659.
3. M. Casciola, S. Chieli, U. Costantino and A. Peraio, *Solid State Ionics*, 1991, **46**, 53-59.
4. M. Casciola, U. Costantino and A. Calevi, *Solid State Ionics*, 1993, **61**, 245-250.

5. D. J. Jones, J.-M. Leloup, Y. Ding and J. Rozière, *Solid State Ionics*, 1993, **61**, 117-123.
6. H. Mohammed, A. Al-Othman, P. Nancarrow, Y. Elsayed and M. Tawalbeh, *Int. J. Hydrogen Energy*, 2021, **46**, 4857-4869.
7. Q. Chen, X. Wang, Z. Wang, J. Cao, J. Dai, J. Wang, E. Fatima-Ezzahra and X. Huang, *ACS Appl. Nano Mater.*, 2022, **5**, 4991-4997.
8. J. Cao, Q. Chen, Z. Wang, X. Wang, Z. Wang, J. Bao and X. Huang, *Sens. Actuators B Chem.*, 2022, **373**, 132713.